Modeling of the Curing Kinetics of No-Flow Underfill in Flip-Chip Applications

Zhuqing Zhang and C. P. Wong, *Fellow, IEEE*

***Abstract*—No-flow underfill has greatly improved the production efficiency of flip-chip process. Due to its unique characteristics, including reaction latency, curing under solder reflow conditions and the desire for no post-cure, there is a need for a fundamental understanding of the curing process of no-flow underfill. Starting with a promising no-flow underfill formulation, this paper seeks to develop a systematic methodology to study and model the curing behavior of this underfill. A differential scanning calorimeter (DSC) is used to characterize the heat flow during curing under isothermal and temperature ramp conditions. A modified autocatalytic model is developed with temperature-dependent parameters. The degree of cure (DOC) is calculated; compared with DSC experiments, the model gives a good prediction of DOC under different curing conditions. The temperature of the printed wiring board (PWB) during solder reflow is measured using thermocouples and the evolution of DOC of the no-flow underfill during the reflow process is calculated. A stress rheometer is used to study the gelation of the underfill at different heating rates. Results show that at high curing temperature, the underfill gels at a lower DOC. Based on the kinetic model and the gelation study, the solder wetting behavior during the eutectic SnPb and lead-free SnAgCu reflow processes is predicted and confirmed by the solder wetting tests.**

***Index Terms*—Coefficient of thermal expansion (CTE), degree of cure (DOC), differential scanning calorimeter (DSC), flip-chip process, no-flow underfill, printed wiring board (PWB).**

I. Introduction

FLIP-CHIP has advantages over other interconnection methods including high input/output (I/O) counts, better electrical performance, high throughput, low profile, etc. [1], and has been practiced in industry for a couple of decades. Recently, the desire for low cost, mass production has resulted in the increasing use of organic substrates such as FR-4 printed wiring board (PWB) instead of ceramic substrates. In order to alleviate the thermal stress on the solder joint caused by the difference between the coefficient of thermal expansions (CTE) of silicon chip and the organic substrate, underfill was invented and its application in flip-chip has greatly enhanced the reliability of the package by redistributing stress among the chip, substrate, underfill and all the solder joints [2], [3]. However, the current underfill process encounters various problems. The conventional underfill is drawn into the gap between the chip and the substrate by the capillary flow, which is usually slow and can be incomplete, resulting in voids. It also produces nonhomogeneity in the resin/filler system. In addition, curing of the underfill takes hours in the oven [4]. These problems are further aggravated with increasing chip dimensions and I/O counts, and decreasing gap distances and pitch sizes.

In order to address the problems associated with conventional underfill, the no-flow underfill process was invented and the first successful no-flow underfill material was developed by Wong and Shi [5]. In the no-flow underfill process, the underfill is dispensed onto the substrate prior to the chip placement. The underfill has the fluxing capability to facilitate the solder to wet on the contact pads of the substrate during solder reflow. This technology simplifies the underfill process by eliminating the flux application and cleaning, underfill dispensing and capillary flow, and combining the solder reflow and underfill curing into one step [6]. The no-flow underfill process and materials have been developed for several years and evaluated in industry. Most no-flow underfill materials are epoxy-based thermosetting resins, which have been widely used as adhesives, surface coatings, molding compounds, etc. However, the curing process of no-flow underfill is unique in that the resin is subjected to the solder reflow with a high-ramped heating and a fast cooling cycle. During the solder reflow process, the resin is fully cured or partially cured. The nature of the no-flow underfill process requires that the underfill have enough reaction latency to maintain its low viscosity until the solder joints are formed. Otherwise, gelled underfill would prevent the melting solders from collapsing onto the contact pads, resulting in low yield of solder joint. On the other hand, elimination of the post cure is desired since post cure takes additional off-line process time, adding to the cost of this process. Hence, the curing procedure of the no-flow underfill is dramatically different from that of the epoxy resins in conventional applications.

This unique process of the no-flow underfill requires a good understanding of the curing behavior of the underfill during the solder reflow process. In order to predict the gelation of the underfill, a suitable curing kinetics needs to be established and the gel point of the underfill needs to be identified. The curing kinetics of the thermosetting resins has been widely studied. The fundamental rate equation which describes the reaction rate as a function of time and temperature is

$$\frac{d\alpha}{dt} = k \bullet f(\alpha) = Ae^{\frac{-E}{RT}} f(\alpha) \tag{1}$$

where α is the degree of cure (DOC) and $(d\alpha)/(dt)$ is the curing rate; k is the rate constant as a function of temperature, generally given by an Arrhenius relation in which E is the activation energy and A is the frequency factor; and $f(\alpha)$ is the reaction model, which is related to the reaction mechanism. The form

Manuscript received June 6, 2002; revised December 6, 2003. This work was supported in part by Resolution Performance Products, Lindau Chemicals, Inc., and Shikoku Chemicals Corporation. This work was recommended for publication by Associate Editor L. T. Nguyen upon evaluation of the reviewers' comments.

The authors are with the School of Materials Science and Engineering, Packaging Research Center, Georgia Institute of Technology, Atlanta, GA 30332 USA (e-mail: cp.wong@mse.gatech.edu).

Digital Object Identifier 10.1109/TCAPT.2004.828556

of $f(\alpha)$ is usually phenomenological. The simplest empirical model used is nth order rate equation:

$$\frac{d\alpha}{dt} = k(1-\alpha)^n \tag{2}$$

where n is the reaction order. The nth order kinetics model predicts a maximum of reaction rate at the beginning of the curing and does not account for any autocatalytic effects. It has been applied to the curing of epoxy resins [7], [8] and maleic polyester resins [9]. More often used as the reaction model is the autocatalytic model shown as

$$\frac{d\alpha}{dt} = k\alpha^m(1-\alpha)^n \tag{3}$$

where m and n are reaction orders. It has been applied to the cure of unsaturated polyester [10] and vinyl ester resins [11].

One drawback of these models is its incapability to deal with diffusion-controlled reaction at the later stage of curing. As the reaction system approaches vitrification, the local viscosity becomes so high that the reaction rate virtually drops to zero. It is possible to modify the autocatalytic model in (3) to provoke mathematically the prediction of zero reaction rate at the vitrification point by using a maximum DOC [12]

$$\frac{d\alpha}{dt} = k\alpha^m(\alpha_{\max}-\alpha)^n \tag{4}$$

where α_{max} is the maximum DOC the reaction system can achieve at a given temperature. Using the above kinetic equations, the isothermal conversion data can be fitted to obtain the model parameters at a given temperature. From the reaction constants at different temperatures, the activation energy and the frequency factor can be obtained. The reaction orders and the maximum DOC can be modeled as functions of temperature to give accurate description to the curing behavior.

In the recent years, the model-free analysis has gained acknowledgment as an approach to analyze the nonisothermal data. The isoconversional method proposed by Friedman allows evaluation of the activation energy unattached to the reaction model [13]. In a constant heating rate experiment, the heating rate is presented by $\beta = dT/dt$. Equation (1) can be represented as

$$\frac{d\alpha}{dT} = \left(\frac{A}{\beta}\right) e^{\frac{-E}{RT}} f(\alpha). \tag{5}$$

Writing (5) in the logarithmic form for different heating rates β_i and considering it at a constant conversion, the following equation can be obtained as the basis of the isoconversional method

$$\ln\left[\beta_i\left(\frac{d\alpha}{dT}\right)_{\alpha,i}\right] = \ln\left[A_\alpha f(\alpha)\right] - \frac{E_\alpha}{RT_{\alpha,i}}. \tag{6}$$

The slope of the plot $\ln[\beta_i(d\alpha/dT)_{\alpha,i}]$ versus $1/T_{\alpha,i}$ gives the activation energy related to a given conversion. Assuming the simple additive superposition of the individual reactions of a possible multistep mechanism, the isoconversional method can be used to predict the curing behavior of isothermal and constant heating rate condition. The model-free analysis allows a conversion-dependent activation energy and is more appropriate than the traditional single activation energy approach for multistep reactions. However, the interpretation of activation energy variation with conversion is still controversial. Even though the isoconversional method allows the prediction of the curing behavior at isothermal temperatures and constant heating rates, it is unable to predict the evolution of DOC under an arbitrary heating profile. In the current study, the no-flow underfill showed a single curing peak, and therefore the traditional isothermal curing kinetics with autocatalytic model is used.

II. Experimental

A. Materials

The no-flow underfill under study was composed of an epoxy resin, a hardener, a latent catalyst, and a fluxing agent. The epoxy in use was EPON Resin 826 from Resolution Performance Products. The hardener was methylhexa-hydrophthalic anhydride (MHHPA) from Lindau Chemicals, Inc. The ratio of epoxy to hardener was 1:0.85 based on the epoxide equivalent weight (EEW) of the epoxy resin and the hydroxyl equivalent weight (HEW) of the hardener. The catalyst was an imidazole derivative from Shikoku Chemicals Corporation. The concentration of the catalyst was 1 phr (per hundred resin). The fluxing agent was incorporated into the no-flow underfill in order to reduce the metal oxide on the solder surface and to facilitate the solder wetting. The fluxing agent in use was hexamethylene glycol from TCI; its concentration was 2.5 wt% based on the mixture of epoxy and hardener. The mixing procedure was as follows. The specified amount of the catalyst was dissolved into the epoxy resin at an elevated temperature ($\sim 90\,^\circ\mathrm{C}$) on a hot plate with magnetic stirring. Then the hardener was added into the mixture and stirred at room temperature. The fluxing agent was mixed into the resin and the whole mixture was stirred at around 70 °C until a uniform solution was formed.

B. Characterization

To study the curing behavior of the no-flow underfill, a modulated differential scanning calorimeter (DSC) by TA Instruments, Model 2920 was used. A sample of about 10 mg was placed into a hermetically sealed DSC sample pan and put in the DSC cell under a 40 ml/min nitrogen purge. The heat flow during curing under isothermal temperatures and constant heating rates was recorded. The constant heating rate curing experiments were conducted from room temperature to 300 °C at 3, 5, 10, 15, and 20 $^\circ\mathrm{C}/\mathrm{min}$. The isothermal curing experiments were carried out at 110, 120, 130, 140, 150, 160, 170, and 180 °C.

To study the viscosity change during the curing of no-flow underfill, a stress rheometer (by TA Instruments, AR1000N) was used in an oscillation mode. A parallel plate geometry was used and the experiments were conducted at a frequency of 1 Hz (for isothermal experiments) or 10 Hz (for constant heating rate experiments) and an oscillation stress of 500 Pa. Temperature-gap compensation was applied to keep constant gap distance of 500 $\mu\mathrm{m}$. The samples were heated from room temperature to 200 $^\circ\mathrm{C}$ at heating rates of 3, 5, 10, 15, and 20 $^\circ\mathrm{C}/\mathrm{min}$. Isothermal curing experiments were conducted at 110, 120, 130,

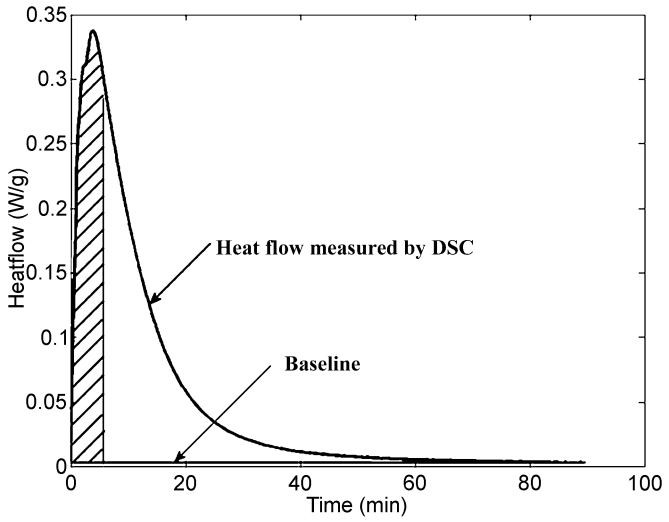

Fig. 1. DSC measured heat flow in an isothermal experiment.

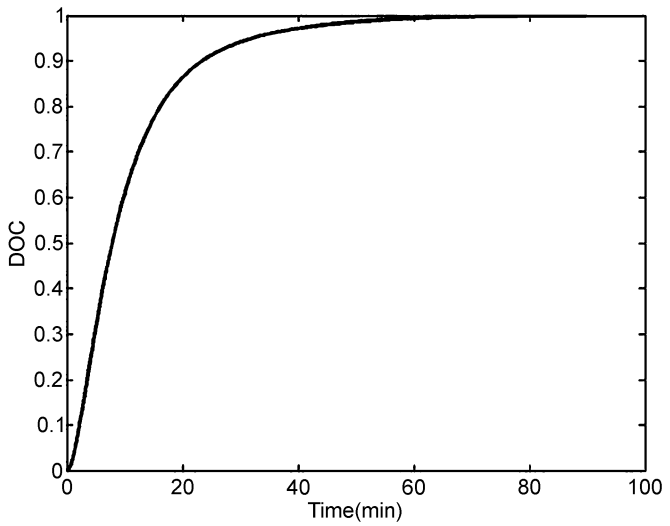

Fig. 2. Calculated DOC versus time in an isothermal experiment.

140, and 150 °C. The gel point is defined point when the phase angle (δ) of the complex viscosity reaches 45°.

C. Reflow Process

The actual temperature profile of the reflow process was obtained according to the thermocouples mounted onto a PWB which was subjected to the reflow process in a seven-zone BTU reflow oven. In order to observe the fluxing capability of the no-flow underfill, a drop of underfill was dispensed onto a cleaned copper sheet placed onto the same PWB. The copper sheets were cleaned by the following procedure: 5 min immersion in acetone, 5 min immersion in methanol, then 20 s immersion in 50/50 $\mathrm{HCl/H_2O}$ solution, followed by DI water rinse and clean air-jet drying. Both the eutectic SnPb solder and the lead-free solder (95.5Sn/3.5Ag/1.0Cu) were used in the reflow test. The solder balls were placed on top of the underfill and the PWB was subjected to the reflow process. The wetting of the solder balls on copper sheet was observed using an optical microscope. To estimate the DOC of the no-flow underfill after reflow, a small amount of the no-flow underfill sealed in a DSC sample pan was placed onto the PWB and reflowed. The DOC of the underfill after reflow was determined by the DSC residual heat under a heating rate of 5 $^\circ\mathrm{C}/\min$.

D. Curing Kinetic Model

The heat flow during curing under isothermal temperatures and constant heating rates was recorded in the DSC experiments. An example of the DSC measured heat flow in an isothermal experiment is illustrated in Fig. 1. The baseline was selected according to the ending heat flow. The area under the heat flow curve was integrated to get the total reaction heat ΔH_{total}. The partial reaction heat $\Delta H(t)$ at time t was calculated by the partial integral as shown in the shaded area. Then the DOC (α) and the reaction rate $(d\alpha/dt)$ at time t were calculated according to (7) and (8). The calculated DOC versus time is shown in Fig. 2. The same method can be used to calculate the DOC in a constant heating rate experiment.

TABLE I
TOTAL REACTION HEAT AT DIFFERENT HEATING RATES IN DSC EXPERIMENTS

Heating rate (°C/min)	Total reaction heat (J/g)
3	320.84
5	312.19
10	326.41
15	320.50
20	322.29
Average	320

The numerical calculations in this study were performed using Matlab 6.5

$$\alpha = \frac{\Delta H(t)}{\Delta H_{total}} \tag{7}$$

$$\frac{d\alpha}{dt} = \frac{\text{heat flow}}{\Delta H_{total}}. \tag{8}$$

The calculated α and $(d\alpha/dt)$ was fitted into the autocatalytic curing kinetic model as shown in (4) using least square method. The kinetic parameters were modeled as functions of the reaction temperature. The DOC change in the isothermal and constant heating experiments was calculated based on the developed kinetic model and was compared to the DSC experiment results. Using the reflow profile measured by thermo-couples, the DOC evolution of the underfill during a solder reflow process was calculated.

III. RESULTS AND DISCUSSION

A. DSC Curing Study

The total reaction heat from the DSC constant heating rate experiments can be integrated and the results are listed in Table I. It can be seen that the total reaction heat does not vary much with the different heating rates. The discrepancies between each run can be attributed to the experimental errors. It can be concluded that the total reaction heat of the curing of the no-flow underfill under this study is around 320 J/g.

The isothermal DSC experiments were carried out at different temperatures from 110 °C to 180 °C. At temperatures lower than 110 °C, the reaction rate was too slow and can be ignored unless the sample stays at this temperature for a long

TABLE II
TOTAL REACTION HEAT AT DIFFERENT ISOTHERMAL TEMPERATURES IN DSC EXPERIMENTS

Isothermal temp. (°C)	Total reaction heat (J/g)
110	287.87
120	288.19
130	311.36
140	326.75
150	318.11
160	307.13
170	304.83
180	292.32

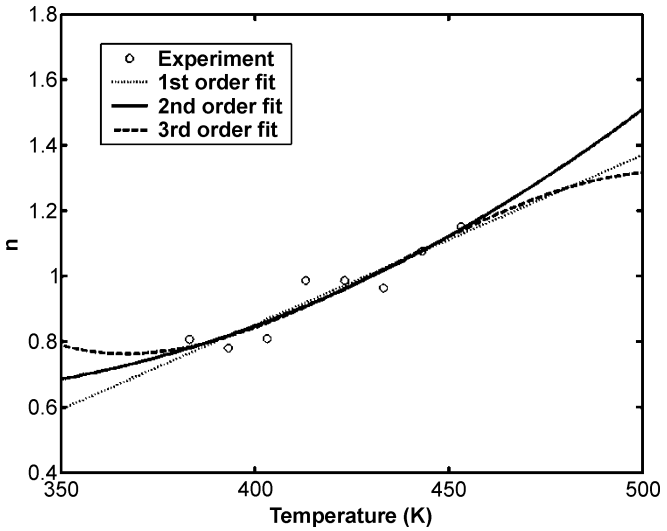

Fig. 3. Reaction order n fitted into polynomial.

time. At high temperatures, significant heat flow losses could occur in the beginning of the experiments when the sample is trying to equilibrate at the isothermal temperature. Table II lists the total reaction heat of the isothermal experiments. As explained early in the paper, at low temperatures, the experiments came to a stop when T_g's of the curing samples approached the isothermal temperatures. So the total reaction heats under those conditions were lower than 320 J/g. From the total reaction heat, the maximum DOC at those temperatures can be calculated. On the other hand, at high temperatures, experimental error was introduced at the initial equilibrium period and total reaction heat was underestimated. However, this does not imply that the maximum DOC decreased with increasing temperature. A treatment for the high temperature data was adopted in this paper where the loss in the total reaction heat was calculated based on the result from the constant heating rate DSC experiments and was used as the initial reaction heat when the DSC started to record heat flow in isothermal experiments. Hence, the maximum DOCs were forced to be 1 for experiments conducted at temperatures equal to or above 150 °C. For reaction temperatures higher than 180 °C, the initial heating introduces too much experimental error and therefore the data were not used for model development.

B. Modeling Results

Using the isothermal DSC data, an autocatalytic model can be established at each isothermal temperature according to (4).

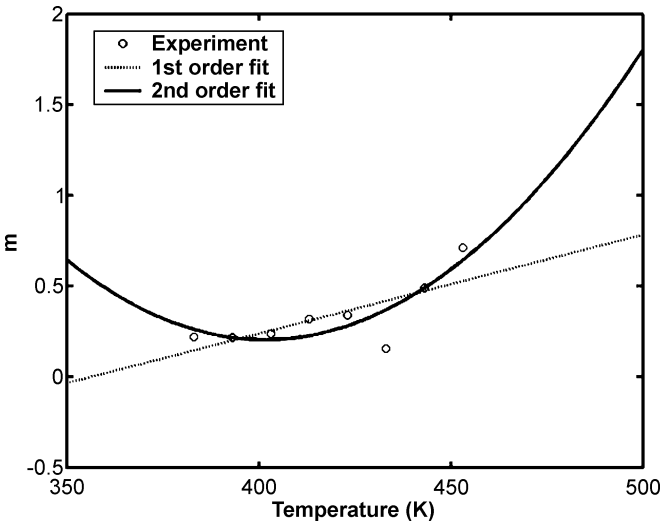

Fig. 4. Reaction order m fitted into polynomial.

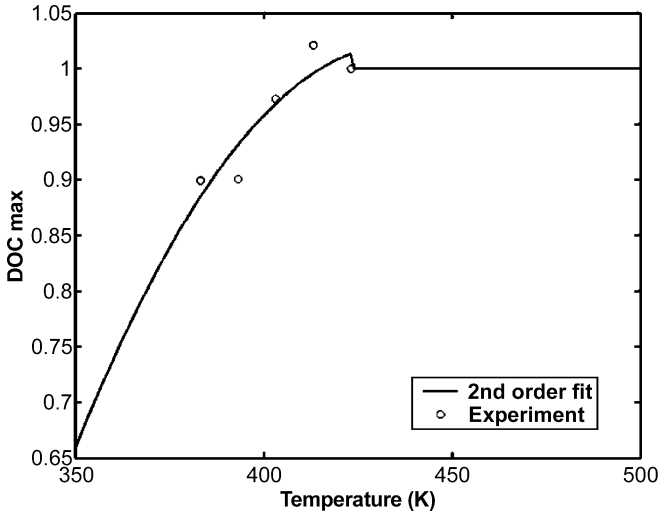

Fig. 5. Maximum DOC as a function of temperature.

The kinetic parameters n, m, and α_{max} are modeled as functions of isothermal temperature in polynomial relations. As can be seen in Fig. 3, n can be fitted into first order, second order, third order, or likewise higher order polynomial relation with the reaction temperature. It also can be observed that although higher order polynomial gives better fit to the present data, it might result in poor prediction for the reaction carried out under temperatures outside the current experiment range. For instance, the third order fit for n predicts a decreasing trend at high temperature. For this reason, the second order polynomial functions were adopted for the parameter n, m, and α_{max} as shown in Figs. 3–5. The maximum DOCs for temperatures higher than 150 °C were forced to be 1 and those for temperatures lower than 150 °C were fitted into a second order polynomial function. The rate constant k is related to the temperature according to the Arrhenius equation as indicated in (1). The activation energy E and the frequency factor A can be obtained in a plot of $\ln k$ versus $1/T$ as shown in Fig. 6.

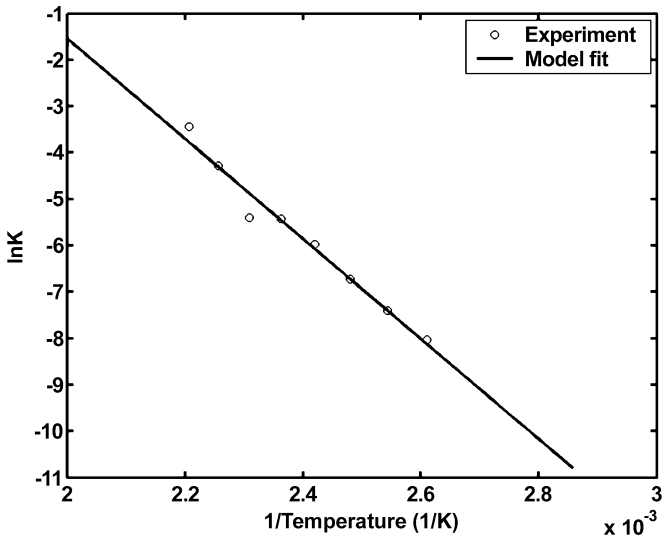

Fig. 6. Plot of lnK versus 1/T.

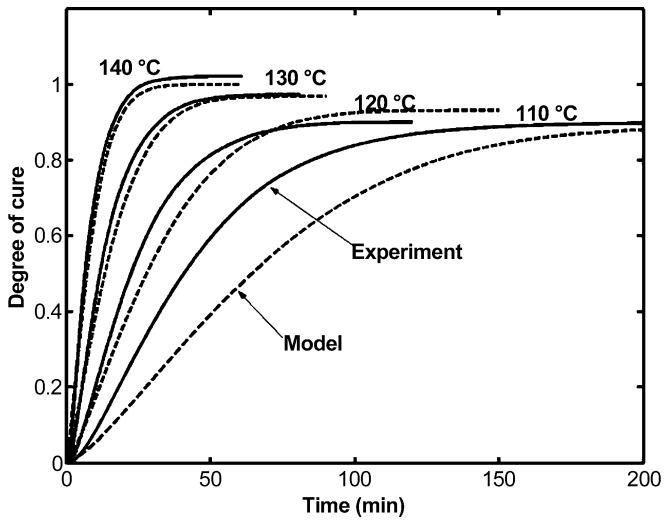

Fig. 7. Comparison of the model and experiment data in isothermal DSC (1).

All the results for the temperature-dependent kinetic parameters are summarized as

$$n = 2.258 \times 10^{-5}T^2 - 0.013\,70T + 2.716$$
$$m = 1.649 \times 10^{-4}T^2 - 0.1324T + 26.80$$
$$\alpha_{\max} = -4.893^{-5}T^2 + 0.042\,66T - 8.279 \quad \text{when } T < 423.15\ K$$
$$\alpha_{\max} = 1 \quad \text{when } T \geq 423.15\ K$$
$$\ln k = \left(-\frac{1.079}{T} + 0.002\,005\right) \times 10^4.$$

Figs. 7 and 8 show the comparison of the calculated DOC from the model and that from the isothermal DSC experiments. It can be seen that at low isothermal temperatures, the model tends to underestimate the reaction rate, especially at the early stage of the reaction. However, at high isothermal temperatures, the model is in pretty good agreement with the experimental data. For the constant heating rate experiments, the modeled

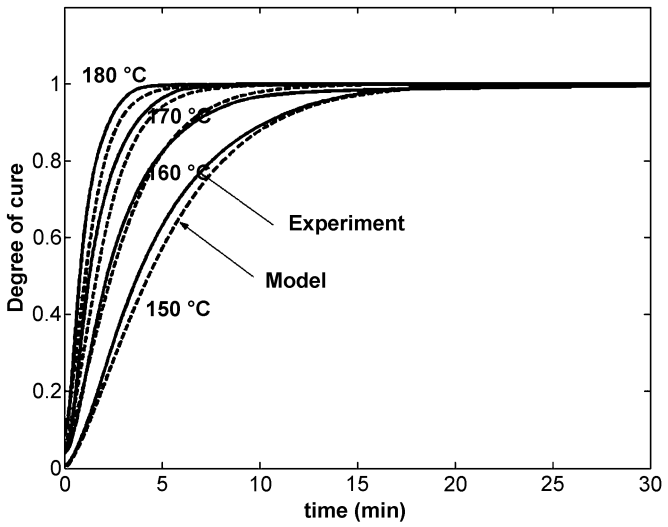

Fig. 8. Comparison of the model and experiment data in isothermal DSC (2).

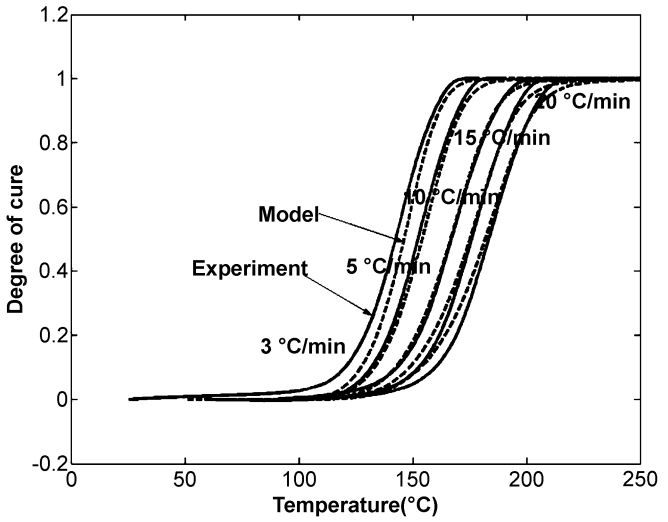

Fig. 9. Comparison of the model and experiment data in constant heating rate DSC.

DOC agrees well with the experimental data as indicated in Fig. 9. To compare this model with the conventionally used autocatalytic kinetic model based on isothermal experiments and B & D (Borchardt and Daniels) kinetic analysis, TA Specialty Library software from TA Instruments was used to obtain the model parameters. The isothermal model (referred as model 2 in Figs. 10 and 11) parameters are

$$\frac{d\alpha}{dt} = k\alpha^m(1-\alpha)^n$$
$$n = 1.23$$
$$m = 0.366$$
$$\ln k = \left(-\frac{9.141}{T} + 0.016\,77\right) \times 10^3.$$

Note that the reaction orders are not temperature-dependent, and α_{max} is always considered to be 1. The B & D kinetic analysis

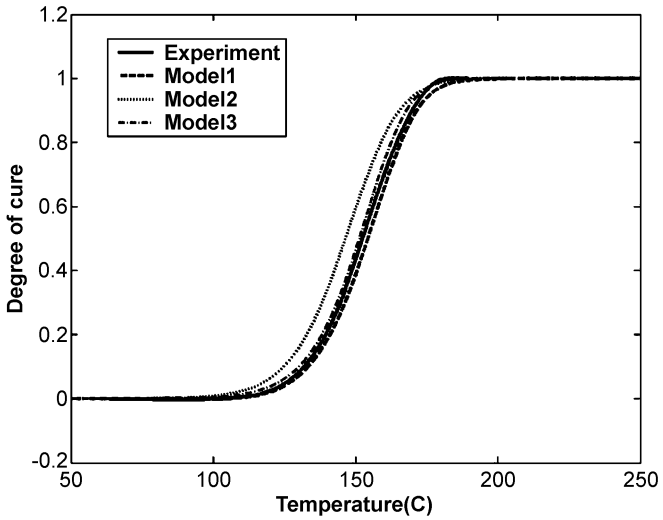

Fig. 10. Comparison of three models with experiment results at a heating rate of 5 °C/ min.

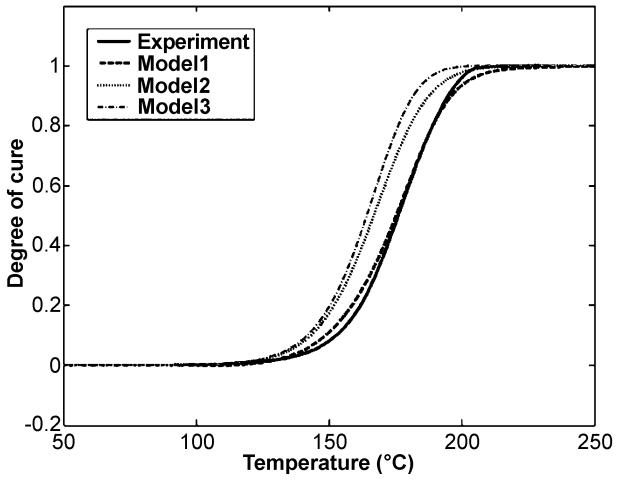

Fig. 11. Comparison of three models with experiment results at a heating rate of 15 °C/ min.

(referred as model 3 in Figs. 10 and 11) uses an n-th order reaction model fitted for DSC data at a constant heating rate of 5 °C/ min

$$\frac{d\alpha}{dt} = k(1-\alpha)^n$$
$$n = 1.24$$
$$\ln k = \left(-\frac{15.011}{T} + 0.030\,17\right) \times 10^3.$$

Figs. 10 and 11 illustrate the difference in the three models in comparison with the experimental data at a constant heating rate of 5 and 15 °C/ min. As can be seen in the two figures, the autocatalytic curing kinetic model with temperature-dependent parameters (model 1) offers the best prediction in the DOC evolution with time. At 5 °C/ min, model 3 gives decent prediction since it uses the DSC data at the same heating rate. However, at a higher ramping rate, neither model 2 nor model 3 shows good agreement with the experimental data while model 1 follows the data very well.

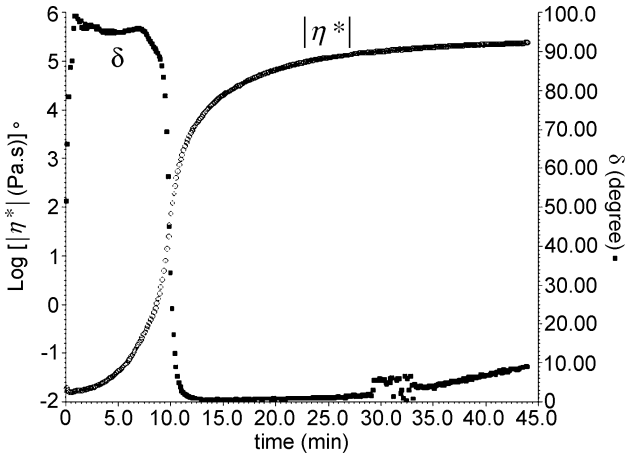

Fig. 12. Isothermal rheology experiment of the no-flow underfill at 130 °C.

TABLE III
DOC AT GELATION AT DIFFERENT ISOTHERMAL TEMPERATURES

Isothermal temp. (°C)	Time to gelation (sec)	DOC at gelation
110	1871	0.39
120	1042	0.39
130	593	0.41
140	218	0.25
150	113	0.19

C. Study of the Gelation of No-Flow Underfill

For no-flow underfill, the time to gelation is most important for achieving high yield in assembly. Beyond the gelation point, the resin is no longer flowable, hence it will interfere with the solder wetting process. In order to correlate the gel point of the underfill with DOC, the change of the underfill viscosity with curing was studied in a stress rheometer in the oscillation mode. Fig. 12 showed the result of the rheometer experiment at an isothermal curing temperature of 130 °C. The figure plots the magnitude of the complex viscosity $(|\eta^*|)$ and the phase angle (δ) for the underfill during the isothermal curing experiment. It can be seen that when the phase angle changes from 90° to 0°, the viscosity of the underfill increases by about six orders of magnitude due to the gelation. Therefore, the time to gel can be obtained for the underfill cured at 130 °C as the phase angle reaches 45°. On the other hand, the DOC of the underfill during the isothermal curing experiment can be calculated from the DSC data as shown in Fig. 2. Based on the time to gel, the DOC at gelation of the underfill during isothermal curing at 130 °C can be determined. Similarly, the rheology experiments can be performed at a constant heating rate and the DOC at gelation at the constant heating rate processes can be obtained.

The isothermal curing experiments of the no-flow underfill at five different temperatures were performed and the time to gelation at each temperature was identified. Compared with the DSC isothermal curing experiments, the DOC at gelation of the underfill at these temperatures is listed in Table III. It can be seen that the DOC at gelation at temperatures around and below 130 °C is around 0.4. However, the DOC at gelation at temperatures higher than 130 °C seems to decrease with increasing temperature. The isothermal curing experiments using the stress rheometer were performed by raising the temperature of the plate to the set temperature and starting the experiment immediately after the set temperature is reached. The initial equilibrium

TABLE IV
DOC AT GELATION AT DIFFERENT HEATING RATES

Heating rate	Temp. at gelation (°C)	DOC at gelation
3 °C/min	133.7	0.28
5 °C/min	142.8	0.26
10 °C/min	156.2	0.26
15 °C/min	163	0.22
20 °C/min	167	0.18

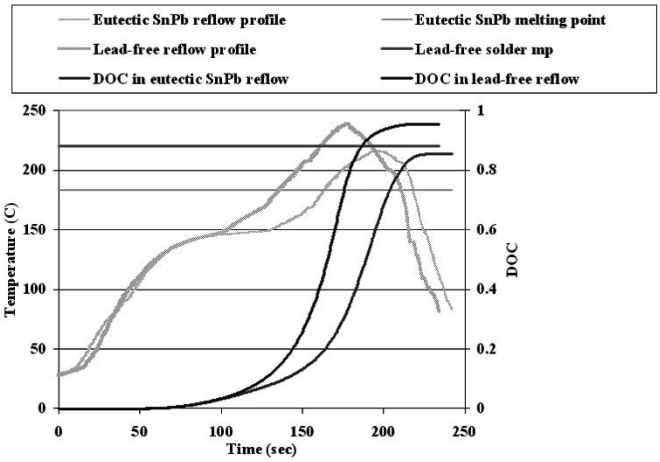

Fig. 13. Reflow profile and evolution of DOC according to the model.

time might introduce some error in the calculation of DOC at gelation. In order to avoid the initial equilibrium error from the isothermal experiment, curing experiments at constant heating rate were conducted to verify the dependency of DOC at gelation on the temperature. Table IV shows the DOC at gelation of the underfill at different heating rates, which was calculated from the DSC curing experiments and rheometer curing experiments. Because the oscillation frequency used in the constant heating rate experiments was higher than that in the isothermal experiments, the gelation appeared to happen at a lower DOC. Despite the difference caused by the frequency, the DOC at gelation showed the same trend. It decreases with increasing heating rate, which is equivalent to high curing temperature. Generally speaking, the gelation is usually considered to happen at a fixed conversion, independent of temperature as long as the reaction mechanism is not a function of temperature [14]. The anomalous gelation behavior of the underfill was studied in detail elsewhere and it was found to be related to the process of network formation [15].

D. Evolution of DOC and Prediction of Gelation in a Reflow Process

The DOC evolution of the no-flow underfill during solder reflow process was calculated according to the developed curing kinetic model and the reflow profiles. Both the eutectic SnPb solder reflow profile and the SnAgCu lead-free solder reflow profile were investigated. The melting point of the eutectic SnPb solder is 183 °C, and the melting point of the lead-free solder is 217 °C. The measured reflow profiles were used as the input to the Matlab program that calculated the DOC of the underfill based on the developed underfill curing kinetic models.

Fig. 13 shows the DOC evolution of the no-flow underfill in the two reflow processes. The melting points of the two types of solder are also marked on the figures. At the temperature

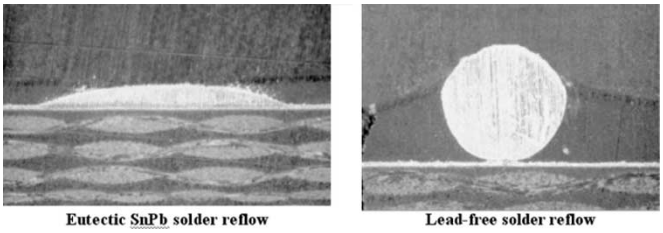

Fig. 14. Wetting of the solder ball on copper sheet after reflow.

TABLE V
COMPARISON OF EXPERIMENT DETERMINED DOC AFTER REFLOW AND MODEL PREDICTION

Total reaction heat (J/g)	Residual heat after reflow (J/g)		Calculated DOC after reflow		Model predicted DOC after reflow	
	SnPb solder reflow	Lead-free solder reflow	SnPb solder reflow	Lead-free solder reflow	SnPb solder reflow	Lead-free solder reflow
320	8.382	1.412	0.974	0.995	0.855	0.954

when the SnPb solder starts to melt, the DOC of the underfill is around 0.2, indicating a low conversion at the solder melting point which is desirable for the application of no-flow underfill. In the lead-free reflow process, on the other hand, the DOC of the underfill is around 0.4 when the lead-free solder starts to melt. According to the study of the gelation behavior, the DOC at gelation varies from 0.2 to 0.4 depending on the curing temperature. Therefore, the underfill should not gel before the solder melting in the eutectic SnPb solder reflow process. On the other hand, in a lead-free solder reflow process, the underfill probably has gelled before the lead-free solder starts to melt. The high viscosity of gelled underfill will restrict the molten solder from wetting on the copper pad. In order to verify the prediction, solder wetting tests were performed. The cross sections of both the eutectic SnPb solder and the lead-free solder balls are shown in Fig. 14. As expected from the kinetic modeling and the gelation study, the eutectic SnPb solder ball can wet on the Cu surface during the eutectic SnPb solder reflow process while the lead-free solder ball cannot wet on the Cu surface in the lead-free solder reflow process.

As a check of the kinetic models, a DSC sample holding the no-flow underfill was taped to the printed circuit board and was subjected to the reflow process. The curing profile of the underfill after reflow was measured using DSC, in which the residual heat of the sample was obtained and used to calculate its DOC after reflow. Table V shows a comparison of the experiment determined DOC after reflow and the prediction of DOC after reflow from the kinetic model. As can be seen from the table, the developed model for curing kinetics tends to underestimate the DOC after reflow in both cases of eutectic SnPb solder reflow and lead-free solder reflow. The discrepancy between the model and the experiments at late stage of reflow process could be due to the thermal transport behavior in the underfill. Unlike in a DSC experiment when the sample is in direct contact with the furnace and the thermal couple, the underfill is in contact with FR4 board that is low in thermal conductivity. During the late stage of reflow process, the board temperature dropped immediately while the temperature inside the underfill sample might remain at a relatively higher temperature for the completion of the reaction. The effect of no-flow underfill curing in the temperature distribution of a flip-chip package was modeled using

FEM analysis and it was found that due to the small volume of the underfill, the exothermic curing reaction did not significantly influence the temperature of the underfill [16]. Therefore, the discrepancy is likely due to limitation of the isothermal curing model. The isothermal data used to develop the model are between 110 °C and 180 °C while the reflow temperature can go up to 220 °C. At high temperatures, the reaction mechanism can be different from that at low temperatures. In consequence, there may be a difference in the reaction order and activation energy that was not accounted for in the current model.

IV. Conclusion

The curing process of no-flow underfill is dramatically different from other thermosetting resins. It has a profound impact on the yield and reliability of a flip-chip on board package. As a phenomenological approach, the curing behavior of a particular no-flow underfill formulation was modeled using an autocatalytic kinetic equation with temperature dependent parameters. Compared with the DSC results, the model gave a good prediction of the evolution of DOC in the isothermal and constant heating rate experiments. The gelation of the no-flow underfill was studied and the gel points at different curing conditions were identified. It was found that the gelation occurs at a lower DOC at a higher curing temperature than it occurs at a lower curing temperature for the underfill in this study. Based on the kinetic model and the temperature profile in the reflow process, the DOC evolution and the gelation of the no-flow underfill was predicted in the eutectic SnPb solder reflow and the lead-free solder reflow processes. Modeling results showed that the no-flow underfill can provide enough curing latency for the wetting of the eutectic SnPb solder while the same underfill would pre-gel in the lead-free solder reflow process before the solder melting. The predicted solder wetting behaviors were confirmed in the solder wetting experiments. The residual reaction heat of reflowed underfill determined by DSC indicated that the model underestimated the DOC after reflow, which was likely to due to the limiting isothermal data.

References

[1] R. R. Tummala, E. J. Rymaszewski, and A. G. Klopfenstein, Eds., *Microelectronics Packaging Handbook*. New York: Chapman & Hall, 1997.

[2] F. Nakano, T. Soga, and S. Amagi, "Resin-insertion effect on thermal cycle resistivity of flip-chip mounted LSI devices," in *Proc. Int. Society of Hybrid Microelectronics Conf.*, 1987, p. 536.

[3] D. Suryanarayana, R. Hsiao, T. P. Gall, and J. M. McCreary, "Flip-chip solder bump fatigue life enhanced by polymer encapsulation," in *Proc. IEEE 40th Electronic Components and Technology Conf.*, 1990, p. 338.

[4] S. Han and K. K. Wang, "Analysis of the flow of encapsulant during underfill encapsulation of flip-chips," *IEEE Trans. Comp., Packag., Manufact. Technol. B*, vol. 20, pp. 424–433, Nov. 1997.

[5] C. P. Wong and S. H. Shi, "No-flow underfill of epoxy resin, anhydride, fluxing agent and surfactant," U.S. Patent 6 180 696, 2001.

[6] C. P. Wong, S. H. Shi, and G. Jefferson, "High performance no-flow underfills for low-cost flip-chip applications: material characterization," *IEEE Trans. Comp., Packag., Manufact. Technol. A*, vol. 21, pp. 450–458, Sept. 1998.

[7] Y. R. Chachad, J. A. Roux, and J. G. Vaughan, "Manufacturing model for three-dimensional irregular pultruded graphite/epoxy composites," *Comp. Part A*, vol. 27A, pp. 201–210, 1996.

[8] S. Suratno, L. Ye, and Y. W. Mai, "Simulation of temperature and curing profiles in pultruded composite rods," *Comp. Sci. Technol.*, vol. 58, pp. 191–197, 1998.

[9] K. Azaar, A. El Brouzi, R. Granger, and J. M. Vergnaud, "Modeling the cure of thermosetting polymers: effect of the coefficient of surface heat transfer," *Plastics Rubber Comp. Process. Applicat.*, vol. 18, pp. 95–102, 1992.

[10] J. M. Salla and X. Ramis, "Comparative study of the cure kinetics of an unsaturated polyester resin using different procedures," *Polymer Eng. Sci.*, vol. 36, p. 835, 1996.

[11] J. H. Lee and J. W. Lee, "Kinetic parameters estimation for cure reaction of epoxy based vinyl ester resin," *Polymer Eng. Sci.*, vol. 34, p. 742, 1994.

[12] V. M. Gonzalez-Romero and N. Casillas, "Isothermal and termperature programmed kinetic studies of thermosets," *Polymer Eng. Sci.*, vol. 29, no. 5, pp. 295–301, 1989.

[13] N. Friedman, "Evaluation of activation energy," *J. Polymer Sci.*, vol. 6C, p. 183, 1963.

[14] P. J. Flory, *Principles of Polymer Chemistry*. Ithaca, NY: Cornell Univ. Press, 1953, ch. IX.

[15] Z. Zhang, E. Beatty, and C. P. Wong, "Study on the curing process and the gelation of epoxy/anhydride system for no-flow underfill for flip-chip applications," *Macromolecular Mater. Eng.*, vol. 288, pp. 365–371, 2003.

[16] Z. Zhang, A. Vorakunpinij, S. Sitaraman, and C. P. Wong, "TTime evolution of temperature distribution of a flip chip no-flow underfill package during solder reflow process," in *Proc. IEEE 53rd Electronic Components and Technology Conf.*, 2003, pp. 443–448.

Zhuqing Zhang received the B.S. degree from Fudan University, Shanghai, China, in 1997 and the M.S. and Ph.D. degrees from the Georgia Institute of Technology (Georgia Tech), Atlanta, in 2001 and 2003, respectively.

She is currently a Post-Doctoral Fellow in the School of Materials Science and Engineering, Georgia Tech.

Dr. Zhang received the Sigma Xi Outstanding M.S. Thesis Award from Georgia Tech in 2002 and the 10th annual Motorola-IEEE/CPMT Society Graduate Student Fellowship for Research in Electronic Packaging for her paper on "Double-Layer No-Flow Underfill Materials and Process" at the 52nd Electronic Components and Technology Conference in San Diego, CA, 2002.

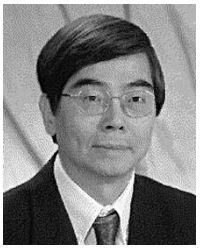

C. P. Wong (SM'87–F'92) received the B.S. degree in chemistry from Purdue University, West Lafayette, IN, and the Ph.D. degree in organic/inorganic chemistry from Pennsylvania State University, University Park.

After his doctoral study, he was awarded two years as a Postdoctoral Scholar at Stanford University, Stanford, CA. He spent 19 years at AT&T Bell Laboratories. He is a Regents Professor with the School of Materials Science and Engineering and a Research Director at the NSF-funded Packaging Research Center, Georgia Institute of Technology, Atlanta. He holds over 40 U.S. patents, numerous international patents, has published over 400 technical papers and 300 key-notes and presentations in the related area. His research interests lie in the fields of polymeric materials, high Tc ceramics, materials reaction mechanism, IC encapsulation, in particular, hermetic equivalent plastic packaging, electronic manufacturing packaging processes, interfacial adhesions, PWB, SMT assembly, and components reliability.

Dr. Wong received the AT&T Bell Laboratories Distinguished Technical Staff Award in 1987, the AT&T Bell Labs Fellow Award in 1992, the IEEE Components, Packaging and Manufacturing Technology (CPMT) Society Outstanding and Best Paper Awards in 1990, 1991, 1994, 1996, and 1998, the IEEE Technical Activities Board Distinguished Award in 1994, the 1995 IEEE CPMT Society's Outstanding Sustained Technical Contribution Award, the 1999 Georgia Tech's Outstanding Faculty Research Program Development Award, the 1999 NSF-Packaging Research Center Faculty of the Year Award, the Georgia Tech Sigma Xi Faculty Best Research Paper Award, the University Press (London, UK) Award of Excellence, the IEEE Third Millennium Medal in 2000, the IEEE EAB Education Award in 2001, the Georgia Tech Distinguished Professor Award in 2004. He was elected a member of the National Academy of Engineering in 2000. He is a Fellow of AIC and AT&T Bell Labs. He served as the Technical Vice President (1990 and 1991), the President (1992 and 1993) of the IEEE-CPMT Society, the IEEE TAB Management Committee (1993–1994), the Chair of the IEEE TAB Design and Manufacturing Committee (1994–1996), the IEEE Nomination and Appointment Committee (1998–1999), and the IEEE Fellow Committee (2001 to the present).